
Using Deep Learning and Macroscopic Imaging of Porcine Heart Valve Leaflets to Predict Uniaxial Stress-Strain Responses

Anonymous Author(s)

Affiliation

Address

email

Abstract

1 Heart valves consist of leaflets that can degrade due to a range of disease processes.
2 To better design prostheses, it is critical to study leaflet mechanics. Although
3 mechanical testing of heart valve leaflets (HVLs) is the standard for evaluating
4 mechanical behavior, imaging and deep learning (DL) networks, such as convolutional
5 neural networks (CNNs), are more readily available and cost-effective. In
6 this work, we determined the influence that a dataset that we curated had on the
7 ability of a CNN to predict the stress-strain response of the leaflets. Our findings
8 indicate that CNNs can be used to predict the polynomial coefficients needed for
9 reconstructing the toe and linear regions of typically observed mechanical behavior,
10 which lie near the physiological strain, 10% strain.

11 **1 Introduction: the importance of heart valves and their mechanical** 12 **characterization**

13 HVLs are arguably one of the most important structures in the heart. They act as one-way valves and
14 prevent oxygenated and deoxygenated blood from mixing Katz [2010]. However, diseases can impact
15 their mechanical properties, so there is a continued pursuit to better mimic natural HVLs, which
16 involves studying their mechanics. However, the standard for acquiring the mechanics of these is
17 through traditional, uniaxial or biaxial mechanical testing Delgadillo et al. [2015], Ross et al. [2020],
18 Lee et al. [1984], which is time-intensive, requires specialized equipment, and often results in the
19 destruction of the samples being tested. Thus, in this work, we first **curated** and tested 51 total HVL
20 samples' images and mechanical data, considered several ground truths by setting different limits on
21 the mechanical data, and finally sought to use DL to predict the stress-strain behavior of HVLs.

22 **1.1 Mechanics of HVLs**

23 Mechanical testing of HVLs involves the application of load in one or two directions on the HVL
24 and observation of the resulting strain. This produces a non-linear stress-strain relationship which
25 mostly consists of a non-linear toe region, a linear transition region, and a plastic region prior to
26 failure Schoen and Levy [1999], Aikawa and Schoen [2014]. Although this behavior is observed in
27 all valves, the prediction of each valve's stress-strain curve from mechanical models is still off or
28 consists of a group average.

29 The resulting mechanics of HVLs arise from their multi-layered structure, however, the tensile
30 properties of the leaflets are dominated by the collagen fibers that run along the circumferential
31 direction of the leaflet Billiar and Sacks [2000], Vesely and Noseworthy [1992]. These are most
32 present in the fibrosa layer, which resides on the aortic side of the leaflet and produces macroscopically
33 visible folds as shown in 1a.

34 1.2 Accessibility and feasibility of needed resources

35 Prior to testing the valve leaflets, these must be extracted from the heart, cut into the appropriate
36 geometry, and a grasping mechanism must be applied carefully so as to not damage the tissue. Then,
37 during testing, the applied load is typically measured through a piezoelectric sensor. This equipment
38 is expensive, requires technical expertise to handle, and must be supervised to ensure proper operation
39 and safety during mechanical tests. Additionally, many samples must be tested in a given time slot
40 since these will go bad if they are not used posthaste. This places an expensive requirement on the
41 investigator’s time and, for these reasons and those above, traditional mechanical testing is not an
42 easily accessible methodology.

43 1.3 Leveraging imaging and deep learning to predict physical properties

44 In contrast, computational resources and imaging are more accessible. Imaging of the HVLs is
45 already used for capturing dimensions and morphological details. Since the fibrosa layer is composed
46 of macroscopically visible collagen fibers, deep learning strategies can be used to predict the resulting
47 mechanical properties from inexpensive imaging methods. In particular, CNNs are one set of
48 algorithms designed to extract features from images to make predictions about the image’s contents.
49 Other works such as Sun et al. [2020], Shen et al. [2021], have been able to predict physical properties
50 from imaging using DL. Thus, in this work, it was determined how our **newly curated dataset**
51 consisting of HVL imaging and mechanical testing impacted the ability of a CNN to reconstruct the
52 stress-strain response of the leaflets. This newly developed dataset is the first of its kind, so far that
53 we are aware.

54 2 Methods

55 2.1 Imaging and mechanical testing of HVLs

56 In this work, porcine HVLs that had been previously fixed in glutaraldehyde were used for imaging
57 and mechanical testing. A Leica stereo microscope was used to capture HVL aortic surface images
58 and a 22N load cell mounted on an Electroforce LM1 TestBench was used to measure the load. Each
59 HVL was cut into a rectangular strip along the circumferential direction; parallel to the direction
60 of the collagen bundles. Prior to testing, thin balsa wooden strips were glued to both ends of the
61 sectioned leaflet for gripping purposes. Finally, HVLs underwent uniaxial tensile testing which
62 consisted of a preconditioning phase to 10% strain at 1Hz for 10 cycles followed by a pull-to-failure
63 phase at 0.1mm/s. This methodology has been extensively used in previous works such as Puperi
64 et al. [2016], Mehta et al. [2018]. The setup can be seen in 1a.

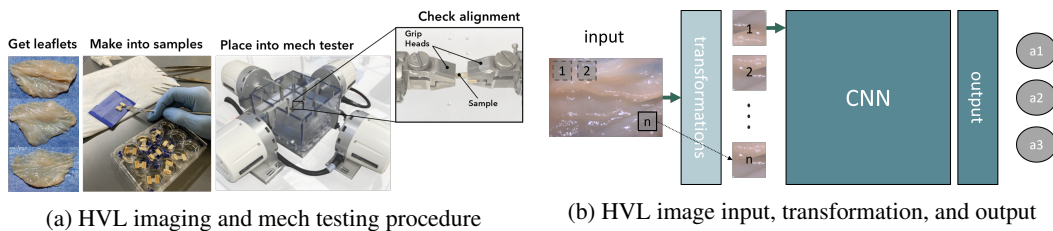


Figure 1: Traditional mechanical testing vs. the proposed CNN framework.

65 2.2 Stress-strain reconstruction using a polynomial

66 The stress-strain curve for every sample is obtained by using stress and strain relationships. Stress is
67 calculated by using $\sigma = F/A$, where σ is the stress, F is the force, and A is the cross-sectional area.
68 Strain is calculated by using $\epsilon = \Delta D/l_g$, where ϵ is the strain, ΔD is the displacement of the moving
69 grip head and l_g is the gauge length of the sample. This data is produced by the mechanical tester as
70 the samples undergo testing, allowing us to readily produce the stress-strain relationship. However,
71 rather than using this continuous data directly with the CNN, we proposed to approximate the curves
72 with a three-degree polynomial and evaluate these through the root-mean-squared error (RMSE).

73 The stress-strain curves of each sample have the characteristic toe (non-linear), linear transition,
74 and yield regions, indicating that a polynomial could effectively approximate the data. This is
75 advantageous because we can then obtain the coefficients, $[a_1, a_2, a_3]$, needed to reconstruct every
76 individual sample's stress-strain curve. Thus, these coefficients are extracted for every sample and
77 we can then use these for training and testing of the CNN.

78 2.3 Data preparation and prediction framework

79 In this work, we created a dataset with 8 samples and another with 51 samples. The input to the CNN
80 consists of RGB HVL sample images, while the ground truth consists of the samples' stress-strain
81 reconstructed curve coefficients. Additionally, we used a data augmentation technique that consisted
82 of creating image patches (224x224) from the original image; each image patch derived from the
83 same image had the same set of coefficients. These image patches were created by specifying the
84 size of a window that served as an image patch's template and then translating it across the original
85 image. After these transformations, the data was ready to be used for training and testing. This work
86 was inspired by that of Liang et al. [2017], however, we used more accessible imaging, focused on
87 the macroscale, and used a different framework.

88 Next, we used three well-known CNN architectures that were pre-trained on ImageNet Deng et al.
89 [2009] since we aimed at having an accessible framework. The CNN architectures that we used were:
90 Alexnet Krizhevsky et al. [2017], VGG11 Simonyan and Zisserman [2014], and Resnet18 He et al.
91 [2016]. We selected these models because they have been extensively used for a variety of tasks in
92 bioengineering, from classification tasks Xue et al. [2016], Chato and Latifi [2017] to composite
93 design Cang et al. [2018], allowing us to focus on the development of our data.

94 Testing also involved image patch transformations on a test sample image, yielding three coefficient
95 values, $[a_1, a_2, a_3]$, for these image patches. The test sample's overall coefficient values were then
96 taken as the mean of each coefficient's value, $[a_{avg1}, a_{avg2}, a_{avg3}]$. The coefficients are predicted by
97 passing the data from the fully-connected layers to a linear layer and these are then evaluated using
98 the mean absolute error (MAE). The mobilization of the data is illustrated in 1b.

99 2.4 Experiments

100 We carried out three experiments to evaluate the influence that our curated dataset and framework
101 had on predicting the coefficients needed for reconstructing a sample's stress-strain curve: **1)** using a
102 smaller set vs. a larger set of samples, 8 and 51, respectively, **2)** using a different strain threshold at
103 which to limit the ground truth data, including hand-picked values near an individual sample's yield,
104 which we refer to as having a "loose" threshold, and **3)** predicting only the linear and quadratic terms
105 rather than also predicting the cubic term. These experiments were chosen to confirm that more data
106 improves performance and to determine the impact on the prediction accuracy as variability in the
107 mechanical data and the reconstructed curves' coefficients are limited.

108 3 Results

109 3.1 Predicted reconstructed curves

110 Stress-strain responses from HVLs are commonly reported up to the physiological strain of 10%
111 in literature Sauren et al. [1983], Arjunon et al. [2013]. In alignment with the second experiment
112 we performed, we varied the strain at which to limit the curve reconstruction using a three-degree
113 polynomial to fit the data. Up to and past the physiological strain, our curve reconstruction scheme
114 had low RMSE, however, incorrect behavior was observed when including data past or near the yield,
115 which we defined with a "loose" threshold through manually picked strain values. Since the RMSE
116 increased the closer and further away we got from the yield, we hypothesized and confirmed through
117 experiment 2 and 3 that our framework would perform better when limiting the data to the toe and
118 transition regions.

119 3.2 Coefficient prediction

120 From the first experiment, we saw an increase in the accuracy of the predicted coefficients, which
121 was expected. For the small set, we had an MAE of 6.88, 4.40, and 6.73 for Alexnet, VGG11,

122 and Resnet18, respectively, while these had an MAE of 3.99, 3.66, and 3.81 for the larger set, see
 123 2a. Although more data is better, mechanical testing is an expensive procedure and our ability to
 124 leverage data augmentation to use the relatively few number of samples in the large set to acquire
 125 good prediction results is optimistic for future work. In the second experiment, we confirmed that
 126 limiting the ground truth data to the toe and linear transition regions improves the accuracy of the
 127 predictions as shown in Table 1. This was further confirmed in experiment 3, where we predicted for
 128 only the linear and quadratic terms as these are capable of capturing the variance from the toe and
 129 linear transition regions in the reconstructed curves. For the case in which 3 terms were predicted,
 130 the MAE was 65.60, 59.05, and 66.75 for Alexnet, VGG11, and Resnet18, respectively, while these
 131 were 3.99, 3.66, and 3.81 when only 2 terms were predicted, see 2b.

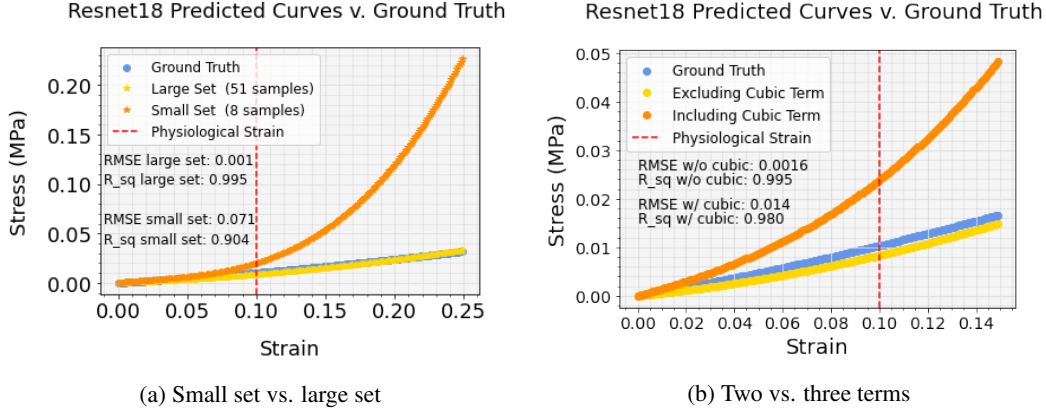


Figure 2: Good alignment between predicted and reconstructed curves in different experiments.

Table 1: High stress-strain variation at higher strain, yielding higher MAE at higher strain thresholds.

| Architecture | Ground Truth Threshold - Strain % | Test MAE |
|--------------|-----------------------------------|-------------|
| Alexnet | 5 | 2.40 |
| VGG11 | 5 | 1.98 |
| Resnet18 | 5 | 1.83 |
| Alexnet | 10 | 3.99 |
| VGG11 | 10 | 3.66 |
| Resnet18 | 10 | 3.81 |
| Alexnet | 15 | 6.97 |
| VGG11 | 15 | 5.34 |
| Resnet18 | 15 | 6.64 |
| Alexnet | Loose | 8.37 |
| VGG11 | Loose | 8.36 |
| Resnet18 | Loose | 7.90 |

132 **4 Conclusion**

133 Through the experiments we performed, we found that CNNs can be used to predict the circumferential
 134 stress-strain response of HVLs from a single image acquired from the sample. We suspect that this
 135 is because macroscopic imaging of the leaflet captures sufficient morphological details related to
 136 the mechanics of the leaflet. Using a larger training set, a strain cap to physiological strain or less,
 137 and limiting predictions to the linear and quadratic terms, we can reduce the MAE of the predicted
 138 coefficients. These results motivate further investigation of the architecture used to form predictions
 139 as well as preparation of the data, since we used a polynomial fit to reconstruct the stress-strain curves
 140 but could explore other models.

141 References

- 142 Arnold M Katz. *Physiology of the Heart*. Lippincott Williams & Wilkins, 2010.
- 143 Jorge O Virues Delgadillo, Sebastien Delorme, Francis Thibault, Robert DiRaddo, Savvas G Hatzikiriakos, et al. Large deformation characterization of porcine thoracic aortas: inverse modeling fitting of uniaxial and biaxial tests. *Journal of Biomedical Science and Engineering*, 8(10):717, 2015.
- 146 Colton J Ross, Devin W Laurence, Ming-Chen Hsu, Ryan Baumwart, Yan D Zhao, Arshid Mir, Harold M Burkhart, Gerhard A Holzapfel, Yi Wu, and Chung-Hao Lee. Mechanics of porcine heart valves' strut chordae tendineae investigated as a leaflet–chordae–papillary muscle entity. *Annals of biomedical engineering*, 48(5):1463–1474, 2020.
- 150 J Michael Lee, David W Courtman, and Derek R Boughner. The glutaraldehyde-stabilized porcine aortic valve xenograft. i. tensile viscoelastic properties of the fresh leaflet material. *Journal of biomedical materials research*, 18(1):61–77, 1984.
- 153 Frederick J Schoen and Robert J Levy. Tissue heart valves: current challenges and future research perspectives. *Journal of Biomedical Materials Research: An Official Journal of The Society for Biomaterials, The Japanese Society for Biomaterials, and The Australian Society for Biomaterials and the Korean Society for Biomaterials*, 47(4):439–465, 1999.
- 157 Elena Aikawa and Frederick J Schoen. Calcific and degenerative heart valve disease. In *Cellular and molecular pathobiology of cardiovascular disease*, pages 161–180. Elsevier, 2014.
- 159 Kristen L Billiar and Michael S Sacks. Biaxial mechanical properties of the native and glutaraldehyde-treated aortic valve cusp: part ii—a structural constitutive model. *Journal of biomechanical engineering*, 122(4):327–335, 2000.
- 162 Ivan Vesely and Ronald Noseworthy. Micromechanics of the fibrosa and the ventricularis in aortic valve leaflets. *Journal of biomechanics*, 25(1):101–113, 1992.
- 164 Yixuan Sun, Imad Hanhan, Michael D Sangid, and Guang Lin. Predicting mechanical properties from microstructure images in fiber-reinforced polymers using convolutional neural networks. *arXiv preprint arXiv:2010.03675*, 2020.
- 167 Sabrina Chin-yun Shen, Marta Peña Fernández, Gianluca Tozzi, and Markus J Buehler. Deep learning approach to assess damage mechanics of bone tissue. *Journal of the Mechanical Behavior of Biomedical Materials*, 123:104761, 2021.
- 170 Daniel S Puperi, Alysha Kishan, Zoe E Punske, Yan Wu, Elizabeth Cosgriff-Hernandez, Jennifer L West, and K Jane Grande-Allen. Electrospun polyurethane and hydrogel composite scaffolds as biomechanical mimics for aortic valve tissue engineering. *ACS Biomaterials Science & Engineering*, 2(9):1546–1558, 2016.
- 174 Shail Maharshi Mehta, Tao Jin, Ilinca Stanciulescu, and K Jane Grande-Allen. Engineering biologically extensible hydrogels using photolithographic printing. *Acta Biomaterialia*, 75:52–62, 2018.
- 177 Liang Liang, Minliang Liu, and Wei Sun. A deep learning approach to estimate chemically-treated collagenous tissue nonlinear anisotropic stress-strain responses from microscopy images. *Acta biomaterialia*, 63:227–235, 2017.
- 180 Jia Deng, Wei Dong, Richard Socher, Li-Jia Li, Kai Li, and Li Fei-Fei. Imagenet: A large-scale hierarchical image database. In *2009 IEEE conference on computer vision and pattern recognition*, pages 248–255. Ieee, 2009.
- 183 Alex Krizhevsky, Ilya Sutskever, and Geoffrey E Hinton. Imagenet classification with deep convolutional neural networks. *Communications of the ACM*, 60(6):84–90, 2017.
- 185 Karen Simonyan and Andrew Zisserman. Very deep convolutional networks for large-scale image recognition. *arXiv preprint arXiv:1409.1556*, 2014.

- 187 Kaiming He, Xiangyu Zhang, Shaoqing Ren, and Jian Sun. Deep residual learning for image
188 recognition. In *Proceedings of the IEEE conference on computer vision and pattern recognition*,
189 pages 770–778, 2016.
- 190 Di-Xiu Xue, Rong Zhang, Hui Feng, and Ya-Lei Wang. Cnn-svm for microvascular morphological
191 type recognition with data augmentation. *Journal of medical and biological engineering*, 36(6):
192 755–764, 2016.
- 193 Lina Chato and Shahram Latifi. Machine learning and deep learning techniques to predict overall
194 survival of brain tumor patients using mri images. In *2017 IEEE 17th international conference on*
195 *bioinformatics and bioengineering (BIBE)*, pages 9–14. IEEE, 2017.
- 196 Ruijin Cang, Hechao Li, Hope Yao, Yang Jiao, and Yi Ren. Improving direct physical properties
197 prediction of heterogeneous materials from imaging data via convolutional neural network and a
198 morphology-aware generative model. *Computational Materials Science*, 150:212–221, 2018.
- 199 AAHJ Sauren, MC Van Hout, AA Van Steenhoven, FE Veldpaus, and JD Janssen. The mechanical
200 properties of porcine aortic valve tissues. *Journal of biomechanics*, 16(5):327–337, 1983.
- 201 Sivakkumar Arjunon, Swetha Rathan, Hanjoong Jo, and Ajit P Yoganathan. Aortic valve: mechanical
202 environment and mechanobiology. *Annals of biomedical engineering*, 41(7):1331–1346, 2013.